

1 **SARS-CoV-2 mutations acquired in mink reduce antibody-mediated**
2 **neutralization**

3
4 Markus Hoffmann,^{1,2,7,*} Lu Zhang,^{1,2,7} Nadine Krüger,¹ Luise Graichen,¹ Hannah Kleine-
5 Weber,^{1,2} Heike Hofmann-Winkler,¹ Amy Kempf,^{1,2} Stefan Nessler,³ Joachim Riggert,⁴ Martin
6 Sebastian Winkler,⁵ Sebastian Schulz,⁶ Hans-Martin Jäck,⁶ Stefan Pöhlmann,^{1,2,8,*}

7
8 Affiliations:

9 ¹Infection Biology Unit, German Primate Center – Leibniz Institute for Primate Research,
10 Göttingen, Germany.

11 ²Faculty of Biology and Psychology, University Göttingen, Göttingen, Germany.

12 ³Institute of Neuropathology, University Medical Center Göttingen, Göttingen, Germany.

13 ⁴Department of Transfusion Medicine, University Medical Center Göttingen, Göttingen,
14 Germany

15 ⁵Department of Anaesthesiology, University of Göttingen Medical Center, Göttingen, Georg-
16 August University of Göttingen, Germany

17 ⁶Division of Molecular Immunology, Department of Internal Medicine 3, Friedrich-Alexander
18 University of Erlangen-Nürnberg, Erlangen, Germany

19 ⁷These authors contributed equally

20 ⁸Lead contact

21 *Correspondence: mhoffmann@dpz.eu (M.H.), spoehlmann@dpz.eu (S.P.)

22

23

24

25 **SUMMARY**

26 **Transmission of SARS-CoV-2 from humans to farmed mink was observed in Europe and**
27 **the US. In the infected animals viral variants arose that harbored mutations in the spike (S)**
28 **protein, the target of neutralizing antibodies, and these variants were transmitted back to**
29 **humans. This raised concerns that mink might become a constant source of human**
30 **infection with SARS-CoV-2 variants associated with an increased threat to human health**
31 **and resulted in mass culling of mink. Here, we report that mutations frequently found in**
32 **the S proteins of SARS-CoV-2 from mink were mostly compatible with efficient entry into**
33 **human cells and its inhibition by soluble ACE2. In contrast, mutation Y453F reduced**
34 **neutralization by an antibody with emergency use authorization for COVID-19 therapy**
35 **and by sera/plasma from COVID-19 patients. These results suggest that antibody responses**
36 **induced upon infection or certain antibodies used for treatment might offer insufficient**
37 **protection against SARS-CoV-2 variants from mink.**

38

39

40

41

42

43

44

45

46

47

48

49 INTRODUCTION

50 The pandemic spread of Severe Acute Respiratory Syndrome Coronavirus 2 (SARS-CoV-2) and
51 the associated disease coronavirus disease 2019 (COVID-19) resulted in 105 million diagnosed
52 infections and 2.3 million deaths ((WHO), 2021). The virus has been introduced into the human
53 population in China in the winter season of 2019, and first cases were detected in the city of
54 Wuhan, Hubei province (Zhou et al., 2020). Bats and pangolins harbor viruses closely related to
55 SARS-CoV-2 and are discussed as sources for SARS-CoV-2 (Lam et al., 2020; Xiao et al., 2020;
56 Zhou et al., 2020). However, it is conceivable that other animals contributed to the spillover of
57 the virus from animals to humans, considering that SARS-CoV was transmitted from bats to
58 humans via civet cats and raccoon dogs (Guan et al., 2003; Lau et al., 2005; Li et al., 2005).

59 The American mink (*Neovison vison*) is farmed in Denmark, the Netherlands and many
60 other countries for its fur. In April 2020, mink in individual farms in the Netherlands developed a
61 respiratory disease and SARS-CoV-2 was detected in the afflicted animals (Molenaar et al., 2020;
62 Oreshkova et al., 2020). Whole-genome sequencing provided evidence that SARS-CoV-2 was
63 initially introduced into mink from humans and that farm workers subsequently acquired the
64 virus from infected animals (Oude Munnink et al., 2020). Further, the data suggested that viruses
65 acquired from infected mink were capable of human-to-human transmission ((Oude Munnink et
66 al., 2020), comments: (Koopmans, 2020; Leste-Lasserre, 2020)). SARS-CoV-2 infection of
67 farmed mink and transmission of the virus from infected animals to humans was subsequently
68 also detected in Denmark and led to the culling of 17 million animals. Finally, apart from the
69 Netherlands and Denmark, also other countries reported SARS-CoV-2 infections of farmed and
70 free-ranging mink, including several European countries (ProMed-mail, 2020a, b, d, e, f) (Fig.
71 1A), Canada (ProMed-mail, 2020g) and the USA (ProMed-mail, 2020c, h).

72 The SARS-CoV-2 spike (S) protein is incorporated into the viral envelope and facilitates
73 viral entry into host cells. For this, the S protein binds to the cellular receptor angiotensin-
74 converting enzyme 2 (ACE2) via its receptor-binding domain (RBD) and employs the cellular
75 serine protease TMPRSS2 for S protein priming (Hoffmann et al., 2020; Zhou et al., 2020). The S
76 protein of SARS-CoV-2 from farmed mink in Denmark and the Netherlands harbors different
77 combinations of mutations relative to SARS-CoV-2 circulating in humans (Oude Munnink et al.,
78 2020) (Fig. 1B and C): A deletion of H69 (H69 Δ) and V70 (V70 Δ) in the S protein N-terminus
79 and amino acid exchanges Y453F in the RBD, I692V located downstream of the furin motif,
80 S1147L in the S2 subunit and M1229I in the transmembrane domain (Fig. 1B and C). Moreover,
81 SARS-CoV-2 containing a combination of five mutations (H69 Δ /V70 Δ /Y453F/I692V/M1229I)
82 in their S protein have been observed, which gave rise to the designation cluster 5 variant. Here,
83 we investigated whether S proteins harboring Y453F either alone or in conjunction with other
84 mutations showed altered expression, host cell interactions and susceptibility to antibody-
85 mediated neutralization.

86

87

88

89

90

91

92

93

94

95

96 **RESULTS**

97 We employed previously described vesicular stomatitis virus-based reporter particles
98 bearing the SARS-CoV-2 S protein to study whether mutations observed in infected mink
99 modulate cell entry and its inhibition (Hoffmann et al., 2020). The S protein from SARS-CoV-2
100 isolate hCoV-19/Wuhan/Hu-1/2019, which harbors an aspartic acid at amino acid position 614
101 (D614) (Korber et al., 2020), was used as control and is subsequently referred to as wildtype
102 (WT). Further, an S protein of identical amino acid sequence but harboring a glycine at position
103 614 (D614G), was used as a reference for S protein variants containing the dominant D614G
104 mutation (Fig. 1D). Finally, S proteins with mutations found in SARS-CoV-2 from mink were
105 analyzed as shown in figure 1D.

106 Immunoblot analysis of S protein-bearing particles revealed that all mutations were
107 compatible with robust particle incorporation of the S protein and cleavage at the furin motif
108 located at the S1/S2 cleavage site (Fig. 1E). Similarly, all S proteins efficiently utilized human
109 ACE2 upon directed expression in otherwise non-susceptible BHK-21 cells (Fig. 2A). Further, all
110 tested S proteins mediated entry into cell lines commonly used for SARS-CoV-2 research (Fig.
111 2B), which were also readily transduced by control particles bearing VSV-G (SI Fig. S1).
112 Substitution D614G, which is dominant in SARS-CoV-2 from humans (Korber et al., 2020) and
113 was also found in viruses from mink, increased the efficiency of S protein-driven entry, as
114 expected (Korber et al., 2020; Plante et al., 2020). Combination of D614G with the mink-specific
115 mutation Y453F (mutant D614G+Y453F) or Y453F in conjunction with H69 Δ , H70 Δ (mutant
116 D614G+H69 Δ /H70 Δ /Y453F) did not modulate entry efficiency when compared to D614G alone
117 (Fig. 2B). Finally, mutation D614G+cluster 5 reduced entry into several cell lines but was
118 compatible with robust entry into the human intestinal cell line Caco-2 and the lung cell line

119 Calu-3 (Fig. 2B). Thus, mutations detected in the S proteins of SARS-CoV-2 from mink were
120 compatible with robust viral entry into human intestinal and lung cells.

121 We next investigated whether mutations observed in SARS-CoV-2 infected mink altered
122 susceptibility of viral entry to inhibition by soluble ACE2 (Monteil et al., 2020) and Camostat, a
123 protease inhibitor active against TMPRSS2 (Hoffmann et al., 2020). Preincubation of particles
124 bearing S protein with soluble ACE2 and preincubation of Calu-3 lung cells with Camostat
125 efficiently blocked entry driven by all S proteins analyzed (Fig 2C and D), with mutant D614G +
126 cluster 5 being particularly sensitive to inhibition by soluble ACE2 (Fig. 2C). In contrast, entry
127 driven by VSV-G was not affected (Fig 2D-E). Thus, mutations acquired in mink may not
128 compromise SARS-CoV-2 inhibition by Camostat and soluble ACE2.

129 A high fraction of convalescent COVID-19 patients exhibits a neutralizing antibody
130 response directed against the S protein that may render most of these patients at least temporarily
131 immune to symptomatic reinfection (Rodda et al., 2020; Wajnberg et al., 2020). Similarly,
132 mRNA-based vaccines induce neutralizing antibodies that play an important role in protection
133 from COVID-19 (Polack et al., 2020; Sahin et al., 2020). Finally, neutralizing monoclonal
134 antibodies are currently being developed for COVID-19 therapy and two have received an
135 emergency use authorization (EUA) for COVID-19 therapy (Baum et al., 2020a; Baum et al.,
136 2020b; Hansen et al., 2020). Therefore, we asked whether S protein mutations found in mink
137 compromise SARS-CoV-2 inhibition by serum or plasma from convalescent COVID-19 patients
138 and neutralizing monoclonal antibodies.

139 We focused our analysis on mutation Y453F, since this mutation is located in the RBD,
140 which constitutes the primary target for neutralizing antibodies. Serum from a control patient
141 failed to inhibit VSV-G or S protein-driven entry (Neg serum #1), as expected. In contrast, 13 out
142 of 14 serum or plasma samples from COVID-19 patients (Pos samples #1-3 and #5-14) potently

143 inhibited S protein but not VSV-G-driven entry while the remaining serum (Pos serum #4) only
144 showed moderate neutralization of S protein-driven entry (Fig. 3A). Importantly, mutation
145 Y453F reduced inhibition by most serum/plasma samples tested, albeit with variable efficiency
146 (median increase of serum/plasma tier required for 50% neutralization [NT50] = 1.62x, range =
147 1.02x to 3.43x), indicating that this RBD mutation may compromise SARS-CoV-2 control by
148 pre-existing neutralizing antibody responses (Fig. 3A and SI Fig. S2). Similarly, the mutation
149 Y453F reduced inhibition by one (Casirivimab/ REGN10933) out of a cocktail of two antibodies
150 with EUA for COVID-19 therapy (REGN-COV2), while an unrelated, non-neutralizing antibody
151 was inactive (IgG1) (Fig. 3B and SI Fig. S3). Finally, the interference of Y453F with entry
152 inhibition by Casirivimab/REGN10933 was in keeping with position 453 being located at the
153 interface of the S protein and the antibody (SI Fig. S4) and with results reported by a previous
154 study (Baum et al., 2020b). Thus, mutation Y453F that arose in infected mink can compromise
155 viral inhibition by human antibodies induced upon SARS-CoV-2 infection or under development
156 for COVID-19 treatment.

157

158

159

160

161

162

163

164

165

166

167 **DISCUSSION**

168 It is believed that SARS-CoV-2 has been introduced into the human population from an
169 animal reservoir, potentially bats or pangolins (Lam et al., 2020; Xiao et al., 2020; Zhou et al.,
170 2020). Furthermore, the virus can replicate in diverse animal species, including cats, tigers, and
171 minks, for which human-to-animal transmission has been reported (Halfmann et al., 2020;
172 McAloose et al., 2020; Molenaar et al., 2020; Oreshkova et al., 2020; Oude Munnink et al., 2020;
173 Segales et al., 2020; Shi et al., 2020). The virus is likely to acquire adaptive mutations that ensure
174 efficient viral spread in these species, for instance by optimizing interactions with critical host
175 cell factors like the entry receptor ACE2. Indeed, mutation Y453F observed in mink may be an
176 adaptation to efficient use of mink ACE2 for entry, since amino acid 453 is known to make direct
177 contact with human ACE2 (Lan et al., 2020; Wang et al., 2020) and mutation Y453F increases
178 human ACE2 binding (Starr et al., 2020). Moreover, viruses bearing Y453F emerged during
179 experimental infection of ferrets and it has been speculated that Y453F might reflect adaptation
180 of the S protein to ferret ACE2 (Everett et al., 2021). Alternatively, Y453F might be the result of
181 viral evasion of the antibody response and a recent report on emergence of Y453F in a patient
182 with long term COVID-19 supports this possibility (Bazykin, 2021).

183 The presence of mutation Y453F alone or in combination with H69 Δ and V70 Δ did not
184 compromise S protein-mediated entry into human cells and its inhibition by soluble ACE2.
185 However, entry into certain cell lines was reduced when Y453F was combined with H69 Δ ,
186 V70 Δ , I692V and M1229I, as found in the S protein of the SARS-CoV-2 cluster 5 variant. This
187 could explain why the cluster 5 variant did not efficiently spread among humans and vanished
188 shortly after its introduction in the human population. The cluster 5 variant S protein was also
189 more sensitive to inhibition by soluble ACE2, hinting towards changes in ACE2 binding affinity
190 when all five signature mutations are present.

191 Y453F markedly reduced the neutralizing potential of an antibody with an emergency use
192 authorization (Casirivimab/REGN10933). Casirivimab/REGN10933 is one out of two antibodies
193 present in the REGN-COV2 antibody cocktail. The other antibody, Imdevimab/REGN10987,
194 targets a different region in the S protein and inhibited S protein-driven entry with high efficiency
195 regardless of the presence of Y453F. In keeping with this finding, a combination of
196 Casirivimab/REGN10933 and Imdevimab/REGN10987 efficiently blocked SARS-CoV-2 with
197 Y453F in cell culture (Baum et al., 2020b). Maybe more concerning is that Y453F diminished
198 entry inhibition by human sera/plasma from convalescent COVID-19 patients. This finding
199 suggests that at least in a fraction of patients antibody responses induced upon infection and
200 potentially also vaccination might provide only incomplete protection against infection with
201 SARS-CoV-2 amplified in mink. In this context it needs to be stated that most serum/plasma
202 samples analyzed completely inhibited entry at the lowest dilution tested, suggesting that
203 individuals that have high antibody titers (induced upon infection or vaccination) might be
204 protected from infection with mink-derived SARS-CoV-2. The transmission of SARS-CoV-2 to
205 wild minks is another alarming observation (ProMed-mail, 2020h), as such transmission events
206 might generate a permanent natural reservoir for such viruses and new emerging variants that
207 could represent a future threat to wildlife and human health.

208 The following limitations of our study need to be considered. We employed pseudotyped
209 particles instead of authentic SARS-CoV-2 and we did not determine whether Y453F affects viral
210 inhibition by T cell responses raised against SARS-CoV-2. Further, we did not investigate whether
211 presence of Y453F in the SARS-CoV-2 S protein increases binding to mink ACE2. Nevertheless,
212 our results suggest that the introduction of SARS-CoV-2 into mink allows the virus to acquire
213 mutations that compromise viral control by the humoral immune response in humans. As a
214 consequence, infection of mink and other animal species should be prevented and it should be

215 continuously monitored whether SARS-CoV-2 amplification in other wild or domestic animals
216 occurs and changes critical biological properties of the virus.

217

218

219

220

221

222

223

224

225

226

227

228

229

230

231

232

233

234

235

236

237

238

239 MATERIALS AND METHODS

240

241 Cell culture

242 All cell lines were incubated at 37 °C in a humidified atmosphere containing 5% CO₂. 293T
243 (human, kidney; ACC-635, DSMZ), Huh-7 (human, liver; JCRB0403, JCRB; kindly provided by
244 Thomas Pietschmann, TWINCORE, Centre for Experimental and Clinical Infection Research,
245 Hannover, Germany) and Vero76 cells (African green monkey, kidney; CRL-1586, ATCC;
246 kindly provided by Andrea Maisner, Institute of Virology, Philipps University Marburg,
247 Marburg, Germany) were cultivated in Dulbecco's modified Eagle medium (DMEM) containing
248 10% fetal bovine serum (FCS, Biochrom), 100 U/ml of penicillin and 0.1 mg/ml of streptomycin
249 (PAN-Biotech). Caco-2 (human, intestine; HTB-37, ATCC) and Calu-3 cells (human, lung;
250 HTB-55, ATCC; kindly provided by Stephan Ludwig, Institute of Virology, University of
251 Münster, Germany) were cultivated in minimum essential medium supplemented with 10% FCS,
252 100 U/ml of penicillin and 0.1 mg/ml of streptomycin (PAN-Biotech), 1x non-essential amino
253 acid solution (from 100x stock, PAA) and 1 mM sodium pyruvate (Thermo Fisher Scientific).
254 A549 cells (human, lung; CRM-CCL-185, ATCC) were cultivated in DMEM/F-12 medium with
255 Nutrient Mix (Thermo Fisher Scientific) supplemented with 10% FCS, 100 U/ml of penicillin
256 and 0.1 mg/ml of streptomycin (PAN-Biotech). In order to obtain 293T, A549 and Calu-3 cells
257 stably expressing human ACE2, cells were transduced with murine leukemia virus-based
258 transduction vectors and subsequently transduced cells were selected with puromycin
259 (Invivogen). Authentication of cell lines was performed by STR-typing, amplification and
260 sequencing of a fragment of the cytochrome c oxidase gene, microscopic examination and/or
261 according to their growth characteristics. Further, cell lines were routinely tested for
262 contamination by mycoplasma.

263

264 **Plasmids**

265 Expression plasmids for vesicular stomatitis virus glycoprotein (VSV-G) (Brinkmann et al.,
266 2017), severe acute respiratory syndrome coronavirus 2 spike glycoprotein (SARS-2-S)
267 containing either a C-terminal HA-epitope tag (SARS-2-S-HA, used for detection in
268 immunoblot) or a truncated cytoplasmic domain (deletion of last 18 amino acid residues at the C-
269 terminus, SARS-2-S Δ 18, used for transduction experiments) (Hoffmann et al., 2020) have been
270 described before. Mink-specific mutations were introduced into the expression plasmids for
271 wildtype SARS-2-S Δ 18 and SARS-2-S-HA by overlap-extension polymerase chain reaction
272 (PCR) and the resulting PCR products were inserted into the pCG1 expression plasmid (kindly
273 provided by Roberto Cattaneo, Mayo Clinic College of Medicine, Rochester, MN, USA) making
274 use of BamHI and XbaI restriction sites.

275 In order to obtain the expression plasmid for delivering ACE2 into cell lines via retroviral
276 transduction, the coding sequence for human ACE2 (NM_001371415.1) was inserted into the
277 pQCXIP plasmid (Brass et al., 2009) making use of NotI and PacI restriction sites. Further, we
278 generated an expression plasmid for soluble ACE2 fused to the Fc-portion of human
279 immunoglobulin G (sol-hACE2-Fc). For this, the sequence coding for the ACE2 ectodomain
280 (amino acid residues 1-733) was PCR-amplified and inserted into the pCG1-Fc plasmid (Sauer et
281 al., 2014) (kindly provided by Georg Herrler, University of Veterinary Medicine, Hannover,
282 Germany) making use of PacI and SalI restriction sites. Sequence integrity was verified by
283 sequencing using a commercial sequencing service (Microsynth Seqlab). 293T cells were
284 transfected by calcium-phosphate precipitation, whereas for transfection of BHK-21 cells
285 Lipofectamine LTX with Plus reagent (Thermo Fisher Scientific) was used.

286

287 **Sequence analysis and protein models**

288 Spike protein sequences from a total of 742 SARS-CoV-2 isolates were retrieved from the
289 GISAID (global initiative on sharing all influenza data) database (<https://www.gisaid.org/>) and
290 analyzed regarding the presence of mink-specific mutations. A summary of the selected S protein
291 sequences, including their GISAID accession numbers, is given in SI-Table. Sequence
292 alignments were performed using the Clustal Omega online tool
293 (<https://www.ebi.ac.uk/Tools/msa/clustalo/>). Protein models were designed using the YASARA
294 (<http://www.yasara.org/index.html>) and UCSF Chimera (version 1.14, developed by the Resource
295 for Biocomputing, Visualization, and Informatics at the University of California, San Francisco)
296 software packages, and are either based on PDB: 6XDG (Hansen et al., 2020) or on a template
297 generated by modelling the SARS-2-S sequence on a published crystal structure (PDB: 6XR8,
298 (Cai et al., 2020)) with the help of the SWISS-MODEL online tool
299 (<https://swissmodel.expasy.org/>).

300

301 **Patient serum and plasma samples**

302 Serum samples were obtained by the Department of Transfusion Medicine of the University
303 Medical Center Göttingen, Göttingen, Germany. Written consent was obtained from all
304 individuals and the study was approved by the local ethics committee (14/8/20). Collection of
305 plasma samples from COVID-19 patients treated at the intensive care unit was approved by the
306 Ethic committee of the University Medicine Göttingen (SeptImmun Study 25/4/19 Ü). Serum and
307 plasma samples were pre-screened for neutralizing activity using SARS-2-S WT pseudotypes, as
308 described below.

309

310 **Production of recombinant human monoclonal antibodies against SARS-CoV-2 spike**

311 VH and VL sequences of Regeneron antibodies Casirivimab/REGN10933,
312 Imdevimab/REGN10987 and REGN10989 (Hansen et al., 2020) were cloned in pCMC3-
313 untagged-NCV (SINO Biologicals, Cat: CV011) and produced in 293T cells by SINO Biological
314 (Beijing, China). The human IgG1 isotype control antibodies IgG1/ κ and IgG1/ λ were produced
315 by transfecting FreeStyle 293-F or 293T cells (Fisher Scientific, Schwerte, Germany, Cat. no.
316 R790-07) with the respective plasmids using the protocol provided with the FreeStyle 293
317 Expression System (Thermo Fisher Scientific, Cat. no. K9000-01). The isotypes contain human
318 V regions from hybridomas that were established from a human HHKLL Trianni mouse (Patent
319 US 2013/0219535 A1). Antibodies were affinity-purified from filtered cultured supernatant on a
320 High-Trap protein G column (GE Healthcare, Chicago, USA, Cat.Nr 17-0404-01).
321 The binding of recombinant antibodies to SARS-2-S was determined by flow cytometry with
322 293T cells stably transfected with plasmid pWHE469-SARS-CoV2 containing the ORF of the
323 spike protein of SARS-CoV-2 isolate Wuhan-Hu-1 (position 21580 – 25400 from GenBank
324 NC_045512) and a GFP reporter plasmid under the control of a doxycycline-inducible promotor
325 (Krueger et al., 2006). Briefly, 293T cells were stained with the recombinant human IgG1
326 antibodies in FACS buffer (PBS with 0.5% bovine serum albumin and 1 nmol sodium azide) for
327 20 minutes in ice, washed, incubated with an Alexa Fluor 647-labeled mouse monoclonal
328 antibody against the human IgG1-Fc (Biolegend, San Diego, USA, cat #409320) and analyzed in
329 a Gallios flow cytometer (Beckman Coulter, Brea, California, USA respectively).

330

331 **Production of rhabdoviral pseudotype particles and transduction of target cells**

332 Rhabdoviral pseudotype particles bearing WT or mutant SARS-2-S, VSV-G or no viral protein
333 (negative control) were prepared according to a published protocol (Kleine-Weber et al., 2019)
334 and involved a replication-deficient VSV vector that lacks the genetic information for VSV-G

335 and instead codes for two reporter proteins, enhanced green fluorescent protein and firefly
336 luciferase (FLuc), VSV* Δ G-FLuc (kindly provided by Gert Zimmer, Institute of Virology and
337 Immunology, Mittelhäusern, Switzerland) (Berger Rentsch and Zimmer, 2011). In brief, 293T
338 cells expressing the desired viral glycoprotein following transfection were inoculated with
339 VSV* Δ G-FLuc and incubated for 1 h at 37 °C before the inoculum was removed and cells were
340 washed. Finally, culture medium was added that was supplemented with anti-VSV-G antibody
341 (culture supernatant from I1-hybridoma cells; ATCC no. CRL-2700; not added to cells
342 expressing VSV-G). Following an incubation period of 16-18 h, pseudotype particles were
343 harvested by collecting the culture supernatant, pelleting cellular debris through centrifugation
344 (2,000 x g, 10 min, room temperature) and transferring aliquots of the clarified supernatant into
345 fresh reaction tubes. Aliquoted pseudotypes were stored at -80 °C until further use.
346 For transduction experiments, target cells were seeded into 96-well plates. The following
347 experimental set-ups were used: (i) In case of experiments comparing the efficiency cell entry by
348 WT and mutant SARS-2-S, target cells were inoculated with 100 μ l/well of the respective
349 pseudotype particles; (ii) For investigation of inhibition of SARS-2-S-driven cell entry by the
350 serine protease inhibitor Camostat mesylate, Calu-3 cells were preincubated for 1 h with medium
351 (50 μ l/well) containing either increasing concentrations of Camostat (0.5, 5 or 50 μ M; Tocris) or
352 dimethyl sulfoxide (solvent control) before the respective pseudotype particles were added on
353 top; in order to assess the ability of sol-hACE2-Fc, patient sera and monoclonal antibodies to
354 block SARS-2-S-driven cell entry, pseudotype particles were preincubated for 30 min with
355 medium containing different dilutions of either sol-hACE2-Fc (1:20, 1:200, 1:2,000) or patient
356 serum/plasma (serum: 1:50, 1:100, 1:200, 1:400, 1:800; plasma: 1:25, 1:100, 1:400, 1:1600,
357 1:6400), or with different concentrations of monoclonal antibody (5, 0.5, 0.05, 0.005, 0.0005
358 μ g/ml), before being inoculated onto Vero76 cells. Pseudotype particles incubated with medium

359 alone served as controls. In all cases, transduction efficiency was analyzed at 16-18 h
360 postinoculation. For this, the culture supernatant was removed and cells were lysed by incubation
361 for 30 min at room temperature with Cell Culture Lysis Reagent (Promega). Next, lysates were
362 transferred into white 96-well plates and FLuc activity was measured using a commercial
363 substrate (Beetle-Juice, PJK) and a Hidex Sense plate luminometer (Hidex).

364

365 **Production of sol-hACE2-Fc**

366 293T cells were grown in a T-75 flask and transfected with 20 µg of sol-hACE2-Fc expression
367 plasmid. At 10 h posttransfection, the medium was replaced and cells were further incubated for
368 38 h before the culture supernatant was collected and centrifuged (2,000 x g, 10 min, 4 °C). Next,
369 the clarified supernatant was loaded onto Vivaspin protein concentrator columns with a
370 molecular weight cut-off of 30 kDa (Sartorius) and centrifuged at 4,000 x g, 4 °C until the sample
371 was concentrated by a factor of 20. The concentrated sol-hACE2-Fc was aliquoted and stored at -
372 80 ° until further use.

373

374 **Analysis of S protein expression, processing and particle incorporation by immunoblot**

375 A total volume of 1 ml of culture medium containing rhabdoviral pseudotypes bearing WT or
376 mutant SARS-2-S-HA were loaded onto a 20% (w/v) sucrose cushion (50 µl) and subjected to
377 high-speed centrifugation (25.000 x g, 120 min, 4°C). As controls, particles bearing no S protein
378 or culture medium alone were used. Following centrifugation, 1 ml of supernatant was removed
379 and the residual volume was mixed with 50 µl of 2x SDS-sample buffer (0.03 M Tris-HCl, 10%
380 glycerol, 2% SDS, 0.2% bromophenol blue, 1 mM EDTA) and incubated at 96 °C for 15 min.
381 Next, samples were subjected to SDS-polyacrylamide gel electrophoresis and proteins were
382 blotted onto nitrocellulose membranes using the Mini Trans-Blot Cell system (Bio-Rad).

383 Following blocking of the membranes by incubation in 5% skim milk solution (skim milk
384 powder dissolved in PBS containing 0.05% Tween-20, PBS-T) for 1 h at room temperature, the
385 membranes were cut in around the 55 kDa marker band of the protein marker (PageRuler
386 Prestained Protein Ladder, Thermo Fisher Scientific). The upper portion of the membrane was
387 probed with anti-HA tag antibody (mouse, Sigma-Aldrich, H3663) diluted 1:1,000 in 5% skim
388 milk solution, while the lower portion of the membrane was probed with anti-VSV matrix protein
389 antibody (Kerafast, EB0011; loading control) diluted 1:2,500 in 5% skim milk solution.
390 Following incubation over night at 4 °C, membranes were washed three times with PBS-T,
391 before being probed with peroxidase-conjugated anti-mouse antibody (Dianova, 115-035-003,
392 1:5,000) for 1 h at room temperature. Thereafter, the membranes were washed again three times
393 with PBS-T, incubated with an in house-prepared developing solution (1 ml of solution A: 0.1 M
394 Tris-HCl [pH 8.6], 250 µg/ml luminol sodium salt; 100 µl of solution B: 1 mg/ml para-
395 hydroxycoumaric acid dissolved in dimethyl sulfoxide [DMSO]; 1.5 µl of 0.3 % H₂O₂ solution)
396 and imaged using the ChemoCam imager along with the ChemoStar Imager Software version
397 v.0.3.23 (Intas Science Imaging Instruments GmbH).

398

399 **Data normalization and statistical analysis**

400 Data analysis was performed using Microsoft Excel as part of the Microsoft Office software
401 package (version 2019, Microsoft Corporation) and GraphPad Prism 8 version 8.4.3 (GraphPad
402 Software). Data normalization was done as follows: (i) In order to assess enhancement of S
403 protein-driven pseudotype entry in BHK-21 cells following directed overexpression of hACE2,
404 transduction was normalized against the assay background (which was determined by using
405 rhabdoviral pseudotypes bearing no viral glycoprotein, set as 1); (ii) To compare efficiency of
406 cell entry driven by the different S protein variants under study, transduction was normalized

407 against SARS-2-S WT (set as 100%); (iii) For experiments investigating inhibitory effects
408 exerted by sol-hACE2-Fc or Camostat Mesylate, patient serum/plasma samples or monoclonal
409 antibodies, transduction was normalized against a reference sample (control-treated cells or
410 pseudotypes, set as 100%). Statistical significance was tested by one- or two-way analysis of
411 variance (ANOVA) with Dunnett's or Sidak's post-hoc test or by paired student's t-test. Only P
412 values of 0.05 or lower were considered statistically significant ($P > 0.05$, not significant [ns]; P
413 ≤ 0.05 , *; $P \leq 0.01$, **; $P \leq 0.001$, ***). Specific details on the statistical test and the error bars
414 are indicated in the figure legends. NT50 (neutralizing titer 50) values, which indicate the
415 serum/plasma titers that lead to a 50% reduction in transduction efficiency, were calculated using
416 a non-linear regression model.

417

418 **SUPPLEMENTAL INFORMATION**

419

420 **SI Table.** Summary of S protein sequences used for analysis and their respective sequence
421 information (related to Figure 1C).

422

423 **Figure S1. Transduction of target cells (related to Figure 2B).**

424 Data presented in Figure 2B were normalized against the assay background (set as 1). Further,
425 transduction efficiency by pseudotype particles bearing VSV-G is shown.

426

427 **Figure S2. Presence of Y453T reduces antibody-mediated neutralization (related to Figure**
428 **3A).**

429 The relative difference in NT50 values between SARS-2-S harboring D614G alone or in
430 conjunction with Y453F was calculated (indicated as Fold difference with SARS-2-S D614G set
431 as 1). The median is indicated by a black line.

432

433 **Figure S3. Flow cytometric detection of antibody-binding to cell-expressed SARS-2-S**
434 **(related to Figure 3B).**

435 293T cells stably transfected with a doxycycline-inducible SARS-2-S (hCoV-19/Wuhan/Hu-
436 1/2019 hCoV-19/Wuhan/Hu-1/2019 isolate) were stained with the indicated Regeneron (REGN)
437 antibodies and an Alexa Fluor 643-conjugated anti-human IgG antibody. A recombinant human
438 IgG served as an isotype control. FI, fluorescence intensity.

439

440 **Figure S4. Y453F centers in the binding interface of antibody REGN10933 and the SARS-2-**
441 **S RBD (related to Figure 3B).**

442 The protein models of the SARS-2-S receptor-binding domain (RBD, blue) in complex with
443 antibodies REGN10933 (purple) and REGN10987 (green) were constructed based on the 6XDG
444 template (Hansen et al., 2020). Residues highlighted in red indicate amino acid position 453 in
445 SARS-2-S RBD (either tyrosine [Y] or phenylalanine [F]).

446

447 **ACKNOWLEDGMENTS**

448 We like to thank Roberto Cattaneo, Georg Herrler, Stephan Ludwig, Andrea Maisner, Thomas
449 Pietschmann and Gert Zimmer for providing reagents and Tobit Steinmetz for the 293T cell line
450 that stably expresses SARS-2-S. Further, we thank Anna-Sophie Moldenhauer, Sara Krause and
451 Manuela Hauke for excellent technical support. We gratefully acknowledge the originating
452 laboratories responsible for obtaining the specimens and the submitting laboratories where

453 genetic sequence data were generated and shared via the GISAID Initiative, on which this
454 research is based. The Pöhlmann lab is supported by BMBF (RAPID Consortium, 01KI1723D
455 and 01KI2006D; RENACO, 01KI20328A, 01KI20396, COVIM consortium). The Jäck lab is
456 supported by grants from the DFG (grants GRK1660 and TRR130), BMBF (COVIM), and the
457 Bavarian Ministry of Science and Art. The Nessler lab is supported by BMBF (Netzwerk
458 Universitätsmedizin, NUM).

459

460 **AUTHOR CONTRIBUTIONS**

461 Conceptualization, M.H., H.-M.J., S.P.; Funding acquisition, S.P.; Investigation, M.H., L.Z.,
462 N.K., L.G., H.K.-W., S.S.; Essential resources, H.H.-W., A.K., M.S.W., S.N., J.R., H.-M.J.;
463 Writing, M.H. and S.P., Review and editing, all authors.

464

465 **DECLARATION OF INTEREST**

466 The authors declare not competing interests

467

468

469

470

471

472

473

474

475

476

477 **REFERENCES**

- 478
- 479 (WHO), W.H.O. (2021). Weekly operational update on COVID-19 - 9 February 2020 (WHO).
- 480 Baum, A., Ajithdoss, D., Copin, R., Zhou, A., Lanza, K., Negron, N., Ni, M., Wei, Y.,
- 481 Mohammadi, K., Musser, B., *et al.* (2020a). REGN-COV2 antibodies prevent and treat SARS-
- 482 CoV-2 infection in rhesus macaques and hamsters. *Science* 370, 1110-1115.
- 483 Baum, A., Fulton, B.O., Wloga, E., Copin, R., Pascal, K.E., Russo, V., Giordano, S., Lanza, K.,
- 484 Negron, N., Ni, M., *et al.* (2020b). Antibody cocktail to SARS-CoV-2 spike protein prevents
- 485 rapid mutational escape seen with individual antibodies. *Science* 369, 1014-1018.
- 486 Bazykin, G.A.S., O.; Danilenko, D; Fadeev, A; Komissarova, K; Ivanova, A; Sergeeva, M.;
- 487 Safina, K; Nabieva, E.; Klink, G.; Garushyants, S.; Zabutova, J.; Kholodnaia, A.; Skorokhod, I.;
- 488 Ryabchikova, V.V.; Komissarov, A.; Lioznov, D. (2021). Emergence of Y453F and Δ 69-70HV
- 489 mutations in a lymphoma patient with long-term COVID-19
- 490 Berger Rentsch, M., and Zimmer, G. (2011). A vesicular stomatitis virus replicon-based bioassay
- 491 for the rapid and sensitive determination of multi-species type I interferon. *PLoS One* 6, e25858.
- 492 Brass, A.L., Huang, I.C., Benita, Y., John, S.P., Krishnan, M.N., Feeley, E.M., Ryan, B.J.,
- 493 Weyer, J.L., van der Weyden, L., Fikrig, E., *et al.* (2009). The IFITM proteins mediate cellular
- 494 resistance to influenza A H1N1 virus, West Nile virus, and dengue virus. *Cell* 139, 1243-1254.
- 495 Brinkmann, C., Hoffmann, M., Lubke, A., Nehlmeier, I., Kramer-Kuhl, A., Winkler, M., and
- 496 Pohlmann, S. (2017). The glycoprotein of vesicular stomatitis virus promotes release of virus-like
- 497 particles from tetherin-positive cells. *PLoS One* 12, e0189073.

498 Cai, Y., Zhang, J., Xiao, T., Peng, H., Sterling, S.M., Walsh, R.M., Jr., Rawson, S., Rits-Volloch,
499 S., and Chen, B. (2020). Distinct conformational states of SARS-CoV-2 spike protein. *Science*
500 *369*, 1586-1592.

501 Everett, H.E., Lean, F.Z.X., Byrne, A.M.P., van Diemen, P.M., Rhodes, S., James, J., Mollett, B.,
502 Coward, V.J., Skinner, P., Warren, C.J., *et al.* (2021). Intranasal Infection of Ferrets with SARS-
503 CoV-2 as a Model for Asymptomatic Human Infection. *Viruses* *13*.

504 Guan, Y., Zheng, B.J., He, Y.Q., Liu, X.L., Zhuang, Z.X., Cheung, C.L., Luo, S.W., Li, P.H.,
505 Zhang, L.J., Guan, Y.J., *et al.* (2003). Isolation and characterization of viruses related to the
506 SARS coronavirus from animals in southern China. *Science* *302*, 276-278.

507 Halfmann, P.J., Hatta, M., Chiba, S., Maemura, T., Fan, S., Takeda, M., Kinoshita, N., Hattori,
508 S.I., Sakai-Tagawa, Y., Iwatsuki-Horimoto, K., *et al.* (2020). Transmission of SARS-CoV-2 in
509 Domestic Cats. *N Engl J Med* *383*, 592-594.

510 Hansen, J., Baum, A., Pascal, K.E., Russo, V., Giordano, S., Wloga, E., Fulton, B.O., Yan, Y.,
511 Koon, K., Patel, K., *et al.* (2020). Studies in humanized mice and convalescent humans yield a
512 SARS-CoV-2 antibody cocktail. *Science* *369*, 1010-1014.

513 Hoffmann, M., Kleine-Weber, H., Schroeder, S., Kruger, N., Herrler, T., Erichsen, S.,
514 Schiergens, T.S., Herrler, G., Wu, N.H., Nitsche, A., *et al.* (2020). SARS-CoV-2 Cell Entry
515 Depends on ACE2 and TMPRSS2 and Is Blocked by a Clinically Proven Protease Inhibitor. *Cell*
516 *181*, 271-280 e278.

517 Kleine-Weber, H., Elzayat, M.T., Wang, L., Graham, B.S., Muller, M.A., Drosten, C., Pohlmann,
518 S., and Hoffmann, M. (2019). Mutations in the Spike Protein of Middle East Respiratory

- 519 Syndrome Coronavirus Transmitted in Korea Increase Resistance to Antibody-Mediated
520 Neutralization. *J Virol* 93.
- 521 Koopmans, M. (2020). SARS-CoV-2 and the human-animal interface: outbreaks on mink farms.
522 *Lancet Infect Dis*.
- 523 Korber, B., Fischer, W.M., Gnanakaran, S., Yoon, H., Theiler, J., Abfalterer, W., Hengartner, N.,
524 Giorgi, E.E., Bhattacharya, T., Foley, B., *et al.* (2020). Tracking Changes in SARS-CoV-2 Spike:
525 Evidence that D614G Increases Infectivity of the COVID-19 Virus. *Cell* 182, 812-827 e819.
- 526 Krueger, C., Danke, C., Pfliederer, K., Schuh, W., Jack, H.M., Lochner, S., Gmeiner, P., Hillen,
527 W., and Berens, C. (2006). A gene regulation system with four distinct expression levels. *J Gene*
528 *Med* 8, 1037-1047.
- 529 Lam, T.T., Jia, N., Zhang, Y.W., Shum, M.H., Jiang, J.F., Zhu, H.C., Tong, Y.G., Shi, Y.X., Ni,
530 X.B., Liao, Y.S., *et al.* (2020). Identifying SARS-CoV-2-related coronaviruses in Malayan
531 pangolins. *Nature* 583, 282-285.
- 532 Lan, J., Ge, J., Yu, J., Shan, S., Zhou, H., Fan, S., Zhang, Q., Shi, X., Wang, Q., Zhang, L., *et al.*
533 (2020). Structure of the SARS-CoV-2 spike receptor-binding domain bound to the ACE2
534 receptor. *Nature* 581, 215-220.
- 535 Lau, S.K., Woo, P.C., Li, K.S., Huang, Y., Tsoi, H.W., Wong, B.H., Wong, S.S., Leung, S.Y.,
536 Chan, K.H., and Yuen, K.Y. (2005). Severe acute respiratory syndrome coronavirus-like virus in
537 Chinese horseshoe bats. *Proc Natl Acad Sci U S A* 102, 14040-14045.
- 538 Leste-Lasserre, C. (2020). Pandemic dooms Danish mink-and mink research. *Science* 370, 754.

539 Li, W., Shi, Z., Yu, M., Ren, W., Smith, C., Epstein, J.H., Wang, H., Crameri, G., Hu, Z., Zhang,
540 H., *et al.* (2005). Bats are natural reservoirs of SARS-like coronaviruses. *Science* 310, 676-679.

541 McAloose, D., Laverack, M., Wang, L., Killian, M.L., Caserta, L.C., Yuan, F., Mitchell, P.K.,
542 Queen, K., Mauldin, M.R., Cronk, B.D., *et al.* (2020). From People to Panthera: Natural SARS-
543 CoV-2 Infection in Tigers and Lions at the Bronx Zoo. *mBio* 11.

544 Molenaar, R.J., Vreman, S., Hakze-van der Honing, R.W., Zwart, R., de Rond, J., Weesendorp,
545 E., Smit, L.A.M., Koopmans, M., Bouwstra, R., Stegeman, A., *et al.* (2020). Clinical and
546 Pathological Findings in SARS-CoV-2 Disease Outbreaks in Farmed Mink (*Neovison vison*). *Vet*
547 *Pathol* 57, 653-657.

548 Monteil, V., Kwon, H., Prado, P., Hagelkruys, A., Wimmer, R.A., Stahl, M., Leopoldi, A.,
549 Garreta, E., Hurtado Del Pozo, C., Prosper, F., *et al.* (2020). Inhibition of SARS-CoV-2
550 Infections in Engineered Human Tissues Using Clinical-Grade Soluble Human ACE2. *Cell* 181,
551 905-913 e907.

552 Oreshkova, N., Molenaar, R.J., Vreman, S., Harders, F., Oude Munnink, B.B., Hakze-van der
553 Honing, R.W., Gerhards, N., Tolsma, P., Bouwstra, R., Sikkema, R.S., *et al.* (2020). SARS-CoV-
554 2 infection in farmed minks, the Netherlands, April and May 2020. *Euro Surveill* 25.

555 Oude Munnink, B.B., Sikkema, R.S., Nieuwenhuijse, D.F., Molenaar, R.J., Munger, E.,
556 Molenkamp, R., van der Spek, A., Tolsma, P., Rietveld, A., Brouwer, M., *et al.* (2020).
557 Transmission of SARS-CoV-2 on mink farms between humans and mink and back to humans.
558 *Science*.

559 Plante, J.A., Liu, Y., Liu, J., Xia, H., Johnson, B.A., Lokugamage, K.G., Zhang, X., Muruato,
560 A.E., Zou, J., Fontes-Garfias, C.R., *et al.* (2020). Spike mutation D614G alters SARS-CoV-2
561 fitness. *Nature*.

562 Polack, F.P., Thomas, S.J., Kitchin, N., Absalon, J., Gurtman, A., Lockhart, S., Perez, J.L., Perez
563 Marc, G., Moreira, E.D., Zerbini, C., *et al.* (2020). Safety and Efficacy of the BNT162b2 mRNA
564 Covid-19 Vaccine. *N Engl J Med*.

565 ProMed-mail (2020a). CORONAVIRUS DISEASE 2019 UPDATE (135): NETHERLANDS
566 (NORTH BRABANT) ANIMAL, FARMED MINK.

567 ProMed-mail (2020b). CORONAVIRUS DISEASE 2019 UPDATE (266): DENMARK
568 (NORTH JUTLAND) ANIMAL, FARMED MINK, FIRST REPORT.

569 ProMed-mail (2020c). CORONAVIRUS DISEASE 2019 UPDATE (366): ANIMAL, USA
570 (UTAH) MINK.

571 ProMed-mail (2020d). CORONAVIRUS DISEASE 2019 UPDATE (468): ANIMAL, SWEDEN,
572 MINK, FIRST REPORT, OIE.

573 ProMed-mail (2020e). CORONAVIRUS DISEASE 2019 UPDATE (490): ANIMAL, GREECE
574 (EM) MINK, FIRST REPORT, OIE, ASSESSMENT.

575 ProMed-mail (2020f). CORONAVIRUS DISEASE 2019 UPDATE (510): ANIMAL, MINK,
576 LITHUANIA, POLAND, FIRST REPORTS, FRANCE, OIE.

577 ProMed-mail (2020g). CORONAVIRUS DISEASE 2019 UPDATE (531): ANIMAL, CANADA
578 (BRITISH COLUMBIA) MINK, OIE.

579 ProMed-mail (2020h). CORONAVIRUS DISEASE 2019 UPDATE (536): ANIMAL, USA
580 (UTAH) WILD MINK, FIRST CASE.

581 Rodda, L.B., Netland, J., Shehata, L., Pruner, K.B., Morawski, P.A., Thouvenel, C.D., Takehara,
582 K.K., Eggenberger, J., Hemann, E.A., Waterman, H.R., *et al.* (2020). Functional SARS-CoV-2-
583 Specific Immune Memory Persists after Mild COVID-19. *Cell*.

584 Sahin, U., Muik, A., Vogler, I., Derhovanessian, E., Kranz, L.M., Vormehr, M., Quandt, J.,
585 Bidmon, N., Ulges, A., Baum, A., *et al.* (2020). BNT162b2 induces SARS-CoV-2-neutralising
586 antibodies and T cells in humans. *medRxiv*, 2020.2012.2009.20245175.

587 Sauer, A.K., Liang, C.H., Stech, J., Peeters, B., Quere, P., Schwegmann-Wessels, C., Wu, C.Y.,
588 Wong, C.H., and Herrler, G. (2014). Characterization of the sialic acid binding activity of
589 influenza A viruses using soluble variants of the H7 and H9 hemagglutinins. *PLoS One* 9,
590 e89529.

591 Segales, J., Puig, M., Rodon, J., Avila-Nieto, C., Carrillo, J., Cantero, G., Terron, M.T., Cruz, S.,
592 Parera, M., Noguera-Julian, M., *et al.* (2020). Detection of SARS-CoV-2 in a cat owned by a
593 COVID-19-affected patient in Spain. *Proc Natl Acad Sci U S A* 117, 24790-24793.

594 Shi, J., Wen, Z., Zhong, G., Yang, H., Wang, C., Huang, B., Liu, R., He, X., Shuai, L., Sun, Z., *et*
595 *al.* (2020). Susceptibility of ferrets, cats, dogs, and other domesticated animals to SARS-
596 coronavirus 2. *Science* 368, 1016-1020.

597 Starr, T.N., Greaney, A.J., Hilton, S.K., Ellis, D., Crawford, K.H.D., Dingens, A.S., Navarro,
598 M.J., Bowen, J.E., Tortorici, M.A., Walls, A.C., *et al.* (2020). Deep Mutational Scanning of

599 SARS-CoV-2 Receptor Binding Domain Reveals Constraints on Folding and ACE2 Binding.

600 *Cell* 182, 1295-1310 e1220.

601 Wajnberg, A., Amanat, F., Firpo, A., Altman, D.R., Bailey, M.J., Mansour, M., McMahon, M.,

602 Meade, P., Mendu, D.R., Muellers, K., *et al.* (2020). Robust neutralizing antibodies to SARS-

603 CoV-2 infection persist for months. *Science* 370, 1227-1230.

604 Wang, Q., Zhang, Y., Wu, L., Niu, S., Song, C., Zhang, Z., Lu, G., Qiao, C., Hu, Y., Yuen, K.Y.,

605 *et al.* (2020). Structural and Functional Basis of SARS-CoV-2 Entry by Using Human ACE2.

606 *Cell* 181, 894-904 e899.

607 Xiao, K., Zhai, J., Feng, Y., Zhou, N., Zhang, X., Zou, J.J., Li, N., Guo, Y., Li, X., Shen, X., *et*

608 *al.* (2020). Isolation of SARS-CoV-2-related coronavirus from Malayan pangolins. *Nature* 583,

609 286-289.

610 Zhou, P., Yang, X.L., Wang, X.G., Hu, B., Zhang, L., Zhang, W., Si, H.R., Zhu, Y., Li, B.,

611 Huang, C.L., *et al.* (2020). A pneumonia outbreak associated with a new coronavirus of probable

612 bat origin. *Nature* 579, 270-273.

613

614

615

616

617

618

619

620

621 **FIGURE LEGENDS**

622

623 **Figure 1. Mink-specific spike protein variants are robustly expressed, proteolytically**
624 **processed and incorporated into viral particles.**

625 (A) European countries that have reported SARS-CoV-2 infection in mink. The mink-specific
626 spike (S) protein mutations under study are highlighted.

627 (B) Summary of mink-specific S protein mutations found in human and mink SARS-CoV-2
628 isolates. Sequences were retrieved from the GISAID (global initiative on sharing all influenza
629 data) database. Legend: a = reference sequences, b = 36/219 sequences carry additional L452M
630 mutation; Abbreviations: *H. sapiens* = *Homo sapiens* (Human), *N. vison* = *Neovison vison*
631 (American Mink), *M. lutreola* = *Mustela lutreola* (European Mink).

632 (C) Location of the mink-specific S protein mutations in the context of the 3-dimensional
633 structure of the S protein.

634 (D) Schematic illustration of the S protein variants under study and their transmission history.
635 Abbreviations: RBD = receptor binding domain, S1/S2 = border between the S1 and S2 subunits,
636 TD = transmembrane domain.

637 (E) Rhabdoviral pseudotypes bearing the indicated S protein variants (equipped with a C-terminal
638 HA-epitope tag) or no viral glycoprotein were subjected to SDS-PAGE under reducing
639 conditions and immunoblot in order to investigate S protein processing and particle
640 incorporation. Detection of vesicular stomatitis virus matrix protein (VSV-M) served as loading
641 control. Black and grey circles indicate bands for unprocessed and processed (cleavage at S1/S2
642 site) S proteins, respectively. Similar results were obtained in four separate experiments.

643

644 **Figure 2. Spike protein variants found in mink enable robust entry into human cells and**
645 **entry is blocked by soluble ACE2 and the protease inhibitor Camostat**

646 (A) Rhabdoviral pseudotypes bearing the indicated S protein variants, VSV-G or no viral
647 glycoprotein were inoculated onto BHK-21 cells previously transfected with empty plasmid or
648 human angiotensin-converting enzyme 2 (hACE2) expression vector.

649 (B) Rhabdoviral pseudotypes bearing the indicated S protein variants, VSV-G (shown in SI
650 Figure 1) or no viral glycoprotein were inoculated onto 293T, 293T (ACE2), Calu-3, Calu-3
651 (ACE2), Caco-2, A549-ACE2, Huh-7 (all human) or Vero76 (non-human primate) cells.

652 (C) Rhabdoviral pseudotypes bearing the indicated S protein variants or VSV-G were
653 preincubated with different dilutions of a soluble hACE2 form fused to the Fc portion of human
654 immunoglobulin G (sol-hACE2-Fc) and subsequently inoculated onto Vero76 cells.

655 (D) Rhabdoviral pseudotypes bearing the indicated S protein variants or VSV-G were inoculated
656 onto Calu-3 cells that were preincubated with different concentrations of Camostat. For all
657 panels: Transduction efficiency was quantified at 16 h postinoculation by measuring the activity
658 of virus-encoded luciferase in cell lysates. Presented are the normalized average (mean) data of
659 three biological replicates, each performed with technical quadruplicates. Error bars indicate the
660 standard error of the mean (SEM). Statistical significance was tested by one- (panels a and b) or
661 two-way (panels c and d) ANOVA with Dunnett's post-hoc test ($P > 0.05$, not significant [ns]; P
662 ≤ 0.05 , *; $P \leq 0.01$, **; $P \leq 0.001$, ***).

663

664 **Figure 3. Y453F reduces neutralization by convalescent sera and monoclonal antibodies**

665 (A) Rhabdoviral pseudotypes bearing the indicated spike (S) protein variants or VSV-G were
666 preincubated with different dilutions of serum (Pos Samples #1-6) or plasma (Pos samples #7-14)
667 from convalescent COVID-19 patients (serum from a healthy individual served as control, Neg

668 Sample) before being inoculated onto Vero76 cells. Transduction efficiency was quantified at 16
669 h postinoculation by measuring the activity of virus-encoded luciferase in cell lysates. The top
670 left panel indicates the serum/plasma titers that lead to a 50% reduction in transduction efficiency
671 (neutralizing titer 50, NT50), which was calculated by a non-linear regression model. Data points
672 from identical serum/plasma samples are connected by lines (grey bars indicate the mean NT50
673 values for all positive samples). Statistical significance of differences in NT50 values between
674 SARS-2-S harboring D614G alone or in conjunction with Y453F was analyzed by paired
675 student's t-test ($P = 0.0212$).

676 (B) The experiment outlined in panel A was repeated using serial dilutions of human monoclonal
677 antibodies. For panels A and B: Presented are the normalized average (mean) data of a single
678 experiment performed with technical quadruplicates. Results were confirmed in a separate
679 experiment (due to limited sample material, only two technical replicates could be analyzed in the
680 confirmatory experiment for the serum samples shown in panel A). Error bars indicate the
681 standard deviation.

682

683

684

685

686

687

688

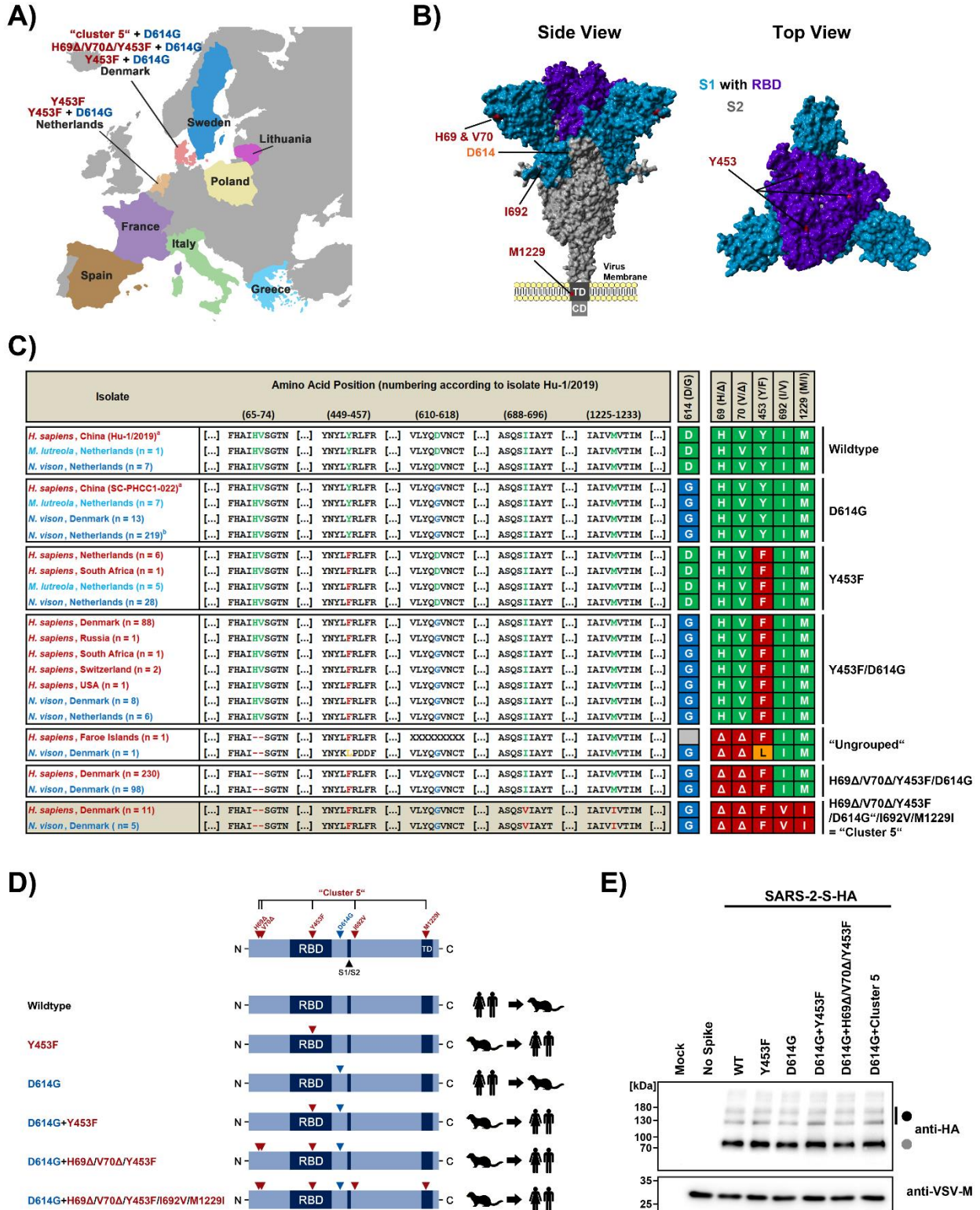
689

690

691

Figure 1

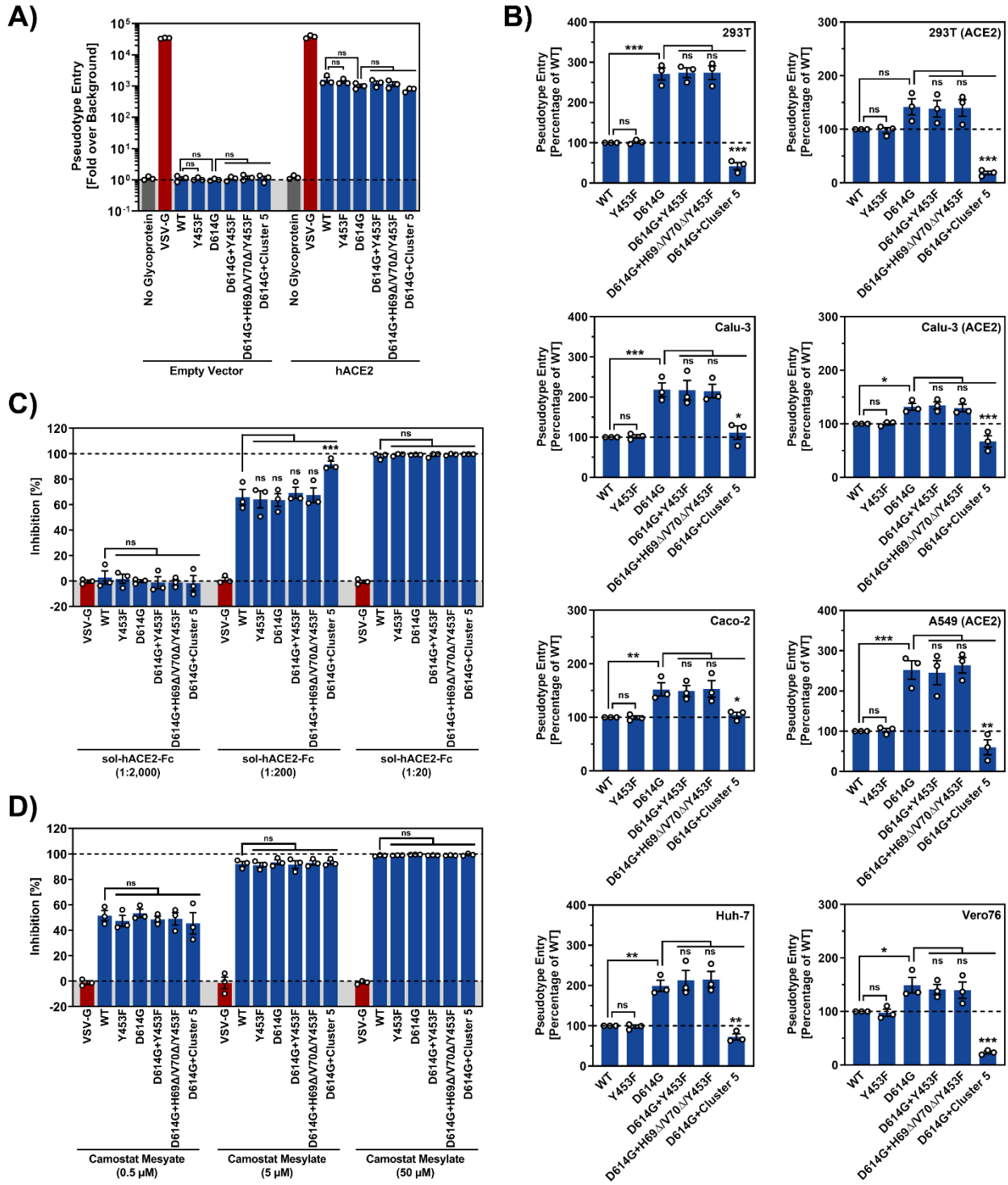
Hoffmann & Zhang et al., 2020



692

693

Figure 2 Hoffmann & Zhang *et al.*, 2020

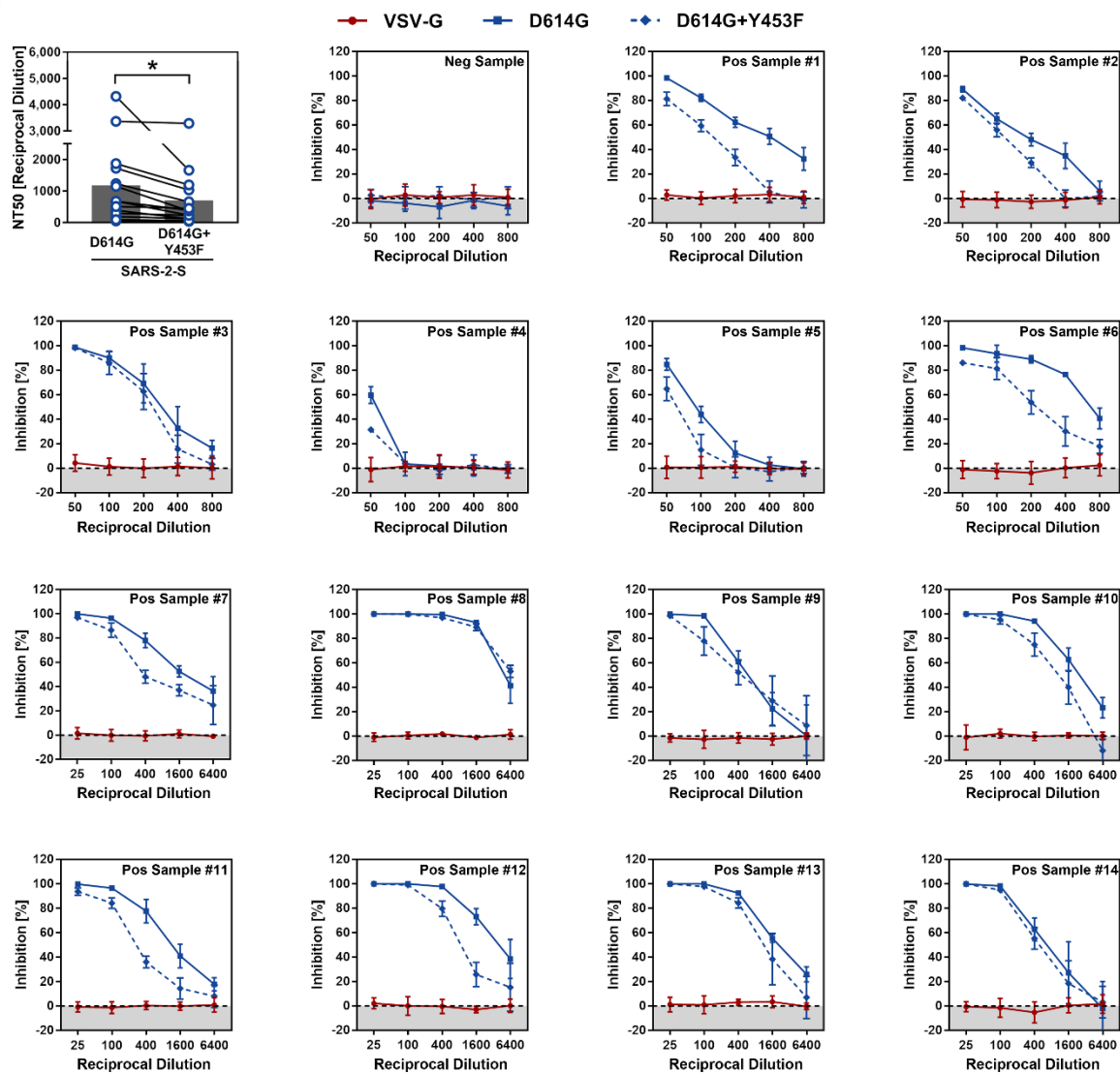


694

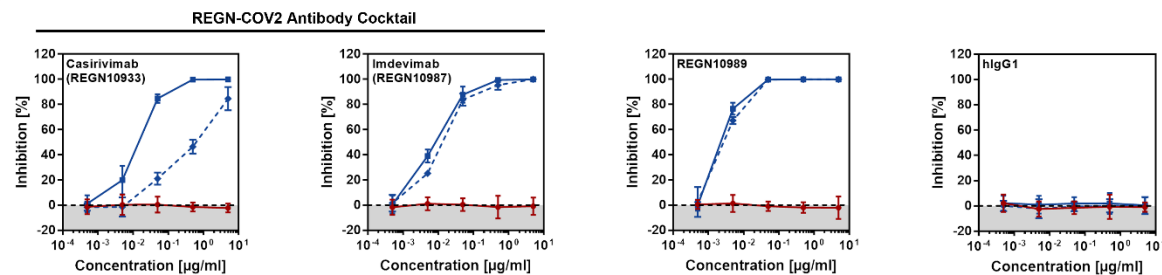
695

Figure 3 Hoffmann & Zhang *et al.*, 2020

A)



B)

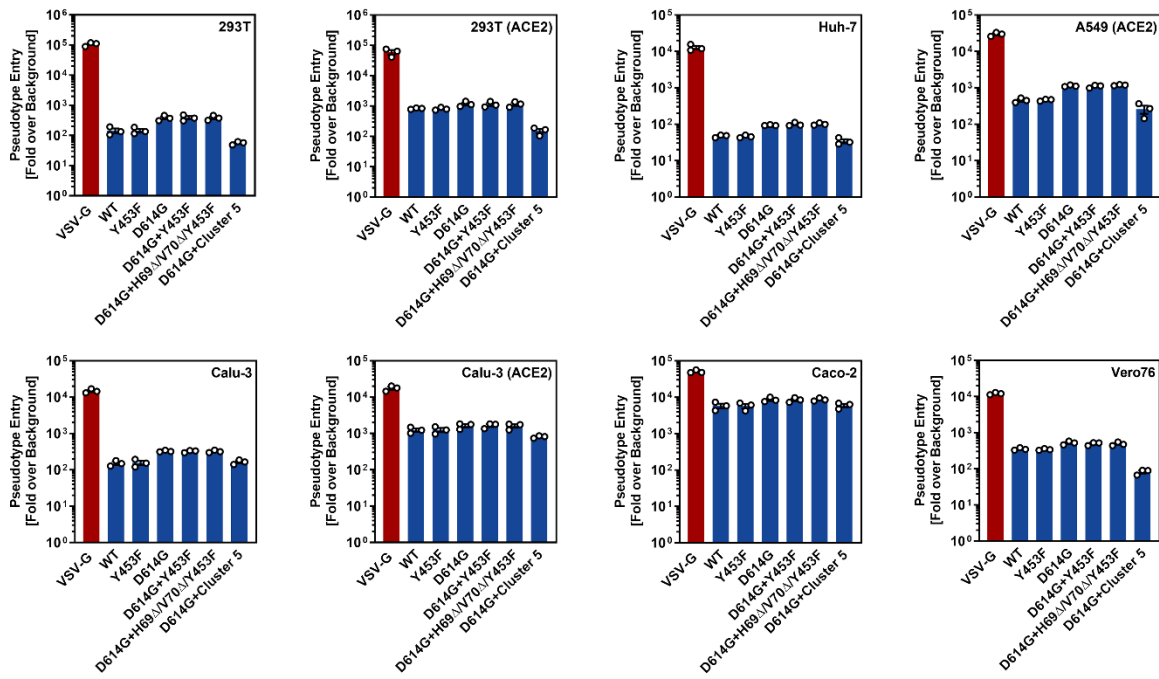


696

697

Figure S1

Hoffmann & Zhang *et al.*, 2020

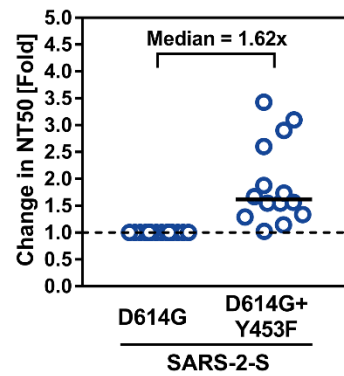


698

699

Figure S2

Hoffmann & Zhang *et al.*, 2020

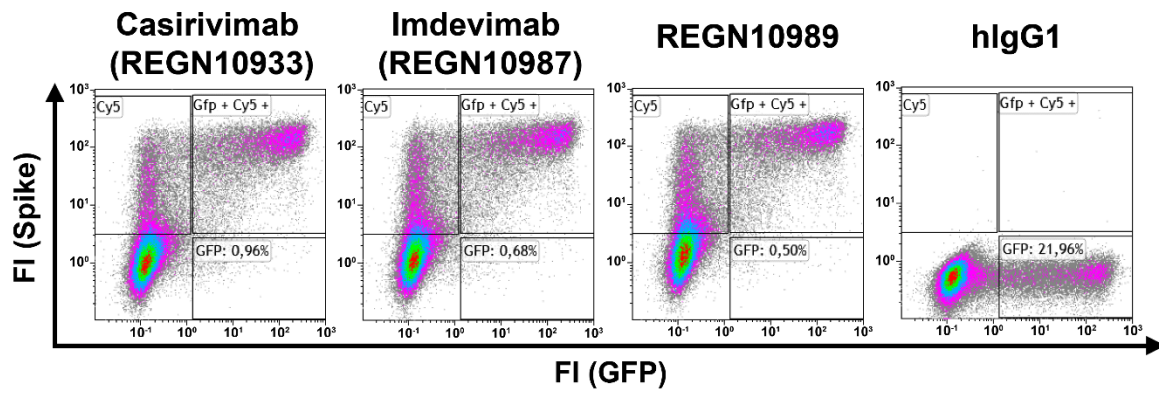


700

701

Figure S3

Hoffmann & Zhang *et al.*, 2020

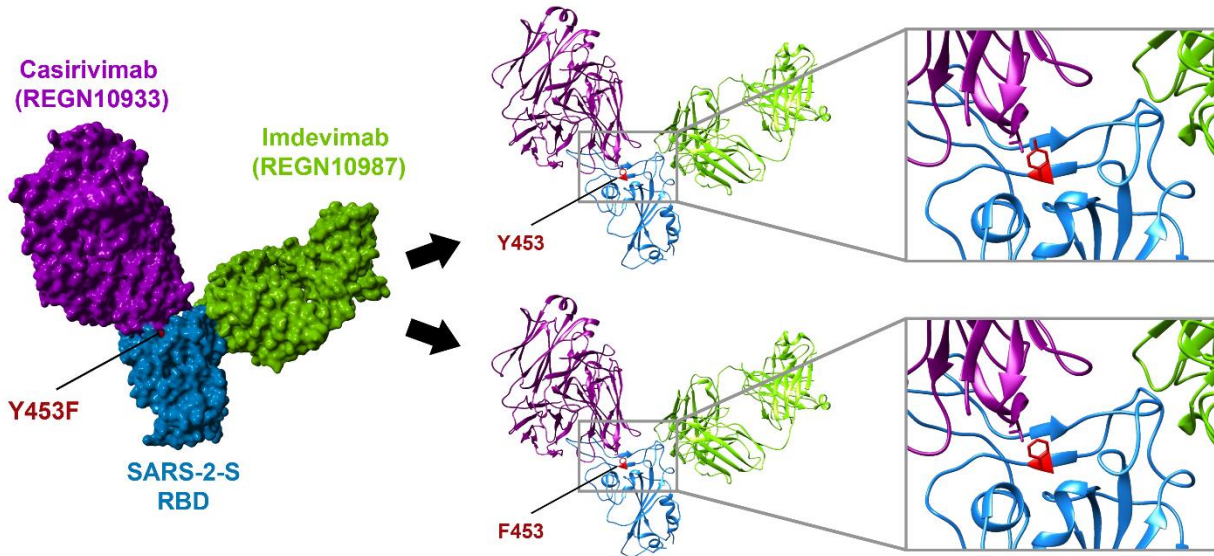


702

703

Figure S4

Hoffmann & Zhang *et al.*, 2020



704

705